Block copolymer directed synthesis of mesoporous TiO_2 for dye-sensitized solar cells

Mihaela Nedelcu,[ab] Jinwoo Lee,[cd] Edward J. W. Crossland,[abe] Scott C. Warren,[c] M. Christopher Orilall,[c] Stefan Guldin,[ab] Sven Hüttner,[ab] Catarina Ducati,[f] Dominik Eder,[f] Ulrich Wiesner,[c] Ullrich Steiner*[ab] and Henry J. Snaith*[g]

Received 30th August 2008, Accepted 14th October 2008
First published as an Advance Article on the web 7th November 2008
DOI: 10.1039/b815166k

The morphology of TiO_2 plays an important role in the operation of solid-state dye-sensitized solar cells. By using polyisoprene-*block*-ethyleneoxide (PI-*b*-PEO) copolymers as structure directing agents for a sol-gel based synthesis of mesoporous TiO_2, we demonstrate a strategy for the detailed control of the semiconductor morphology on the 10 nm length scale. The careful adjustment of polymer molecular weight and titania precursor content is used to systematically vary the material structure and its influence upon solar cell performance is investigated. Furthermore, the use of a partially sp^2 hybridized structure directing polymer enables the crystallization of porous TiO_2 networks at high temperatures without pore collapse, improving its performance in solid-state dye-sensitized solar cells.

1 Introduction

Mesoporous materials[1,2] have a wide range of applications, including their important role in photoelectrochemical cells, photocatalysis, and sensors. Because of its high refractive index and photocatalytic properties, TiO_2 is commercially used as pigments and surface coatings. Since it is mass produced, it is relatively cheap and widely available, which makes it an attractive material to explore future technological applications. In the 1980s TiO_2 was employed in electrochemical photovoltaics, but because of its wide band-gap, no visible light is absorbed directly in the material and optical sensitization is required. At first, this appeared to be a "show-stopper" for integrating wide band-gap oxides into solar cells since only a fraction of the incident light could be absorbed in a monolayer sensitization. Amongst the developments of mesoporous oxides, in 1991, O'Regan and Grätzel discovered that mesoporous films of anatase TiO_2 fabricated from sol-gel processed sintered nanoparticles performed remarkably well when integrated into "dye-sensitized solar cells" (DSCs), and delivered the surface area multiplicity required to absorb the majority of the incident light over the active region of the sensitizer.[3] To describe the operational mechanism: upon light absorption in the sensitizer, an electron is "injected" into the TiO_2 and the resultant oxidized dye molecule is regenerated by an iodide/triiodide redox couple, which carries the holes to the external circuit. Though the liquid electrolyte based cell is reasonably efficient, due to processing and durability issues with liquid electrolytes, solid-state redox couples have been rigorously investigated. In 1998, the DSCs concept was extended by Bach and Grätzel[4] by replacing the liquid electrolyte with an organic hole transporting molecule, 2,2′,7,7′-tetrakis(N,N-di-p-methoxyphenylamine)-9,9′-spirobifluorene (spiro-MeOTAD), which remains the most efficiently operating molecular hole-transporter when incorporated into DSCs, due to its good charge carrier mobility and ability to back-fill mesoporous structures.[5,6]

Both liquid electrolyte and solid-state dye-sensitized solar cells now exhibit excellent power conversion efficiencies of 11% and 5%, respectively.[7] While this makes them a promising future alternative to silicon devices, further improvement of DSCs are possible and clearly necessary, especially for the solid-state cell. The key issues for further development of solid-state DSCs appear to be: (*i*) enhancement of light absorption by the dye, both in terms of molecular extinction and spectral range, (*ii*) improvement of hole-transporter infiltration into mesoporous structures, and (*iii*) the improvement of the physical and electronic properties of the inorganic semiconducting phase, with specific attention to enhanced electron transport, and reduced charge recombination. Control of the mesostructure of the metal oxide is particularly important since it is critical in governing its electronic properties and function in the solar cell (transport and recombination). Further to the mesostructure, the specific crystal structure, surface-state density and electronic structure of surfaces is also central to material optimization. Clearly, effective operation in DSCs is achieved with the present state-of-the-art (*i.e.* the assembly of 10–20 nm sized nanoparticles). However, following 20 years of optimization further improvements are not directly foreseeable and the detailed nature of the mesoporous morphology and electronic characteristics of the material are still far from ideal, even in the best examples. A specific limitation of

[a]*Department of Physics, Cavendish Laboratories, University of Cambridge, Cambridge, UK CB3 OHE*
[b]*University of Cambridge Nanoscience Centre, Cambridge, UK CB3 OFF*
[c]*Department of Materials Science and Engineering, Cornell University, Ithaca, NY, 14853, USA*
[d]*Department of Chemical Engineering, Pohang University of Science and Technology, San 31, Hyo-ja-dong, Pohang, Kyungbuk 790-784, Korea*
[e]*Freiburg Institute for Advanced Studies, Albert-Ludwigs-Universität Freiburg, 79104 Freiburg*
[f]*Department of Materials Science and Metallurgy, University of Cambridge, Cambridge, UK CB2 3QZ*
[g]*Department of Physics, Clarendon Laboratory, University of Oxford, UK OX1 3PU*

the standard nanoparticle approach to fabricating extremely porous films is that the electron transport slows disproportionately as the porosity increases,[8] and for fabricating films with exceptionally large internal surface areas the electron transport slows considerably as the particle size is reduced and the roughness increased.[9]

A promising approach to controlling the morphology on the 10 nm length scale of organic-inorganic hybrid materials is based on self-assembly assisted by block copolymers. The approached was introduced by Wiesner and coworkers,[10] Stucky and coworkers[1,11,13] and Coakley and MeGehee[12] in the late 90s. Inorganic precursors are embedded in one domain of a microphase separated block copolymer morphology. These hybrids can subsequently be transformed into a nanostructured/mesoporous ceramic by calcination of the blend. This was first demonstrated for silica-type materials and subsequently extended to other ceramics. More recently TiO_2 fabricated in this manner has been used very effectively in liquid electrolyte based DSCs.[14] Zukalova *et al.* have demonstrated that block copolymer templated TiO_2 can exhibit superior performance to particle-based mesoporous films when incorporated into thin film liquid electrolyte based DSCs. Improvements were primarily derived from the higher surface area of the structured material. However, the specific route to mesoporous TiO_2 developed by Zukalova *et al.* has a number of limitations: the hydrolytic sol-gel route is highly reactive, limiting the processing window and the ensuing control over mesopore morphology. The chemical reactions are water-based, severely limiting the choice in structure directing polymers and practical thickness of the ensuing films. The specific commercially available Pluronic 123 system previously used may also prove less than ideal for incorporation into solid-state DSCs due to the extremely small pore size (~7 nm) inhibiting efficient molecular hole-transporter infiltration. Further improvements are predicted if the crystallinity of the mesoporous material can be enhanced.[14]

In the past, copolymer-directed TiO_2 synthesis has typically been limited to temperature treatments below 400–450 °C to prevent collapse of the mesoporous structure. The resulting limited crystallinity of TiO_2 annealed at these relatively low temperatures is thought to contribute towards its low electron diffusion coefficient due to a high density of trap sites. The combination of high temperature treatment while maintaining a high porosity has recently been demonstrated by Lee *et al.* employing a combined assembly of soft and hard (CASH) chemistries method.[15] Heating an sp^2 hybridized carbon containing hydrophobic block, such as polyisoprene (PI), under non-oxidizing conditions converts this block into a sturdy amorphous graphitic-like carbon material that acts as a scaffold for the TiO_2 network, preventing its collapse. This enables heat treatments at much higher temperatures without loss of porosity. The carbon is subsequently oxidized away by heating in air at lower temperatures.

Here, we report the first use of mesoporous of TiO_2, fabricated by employing structure directing copolymers, integrated into solid-state dye-sensitized solar cells using spiro-MeOTAD as the hole-transport medium. The TiO_2 synthesis is directed by the polyisoprene-*block*-ethyleneoxide (PI-*b*-PEO) microphase morphology *via* a non-hydrolytic sol-gel route. By systematically tuning the polymer molecular weight and the titania precursor content, we have fine-tuned the TiO_2 morphology on the 10 nm length scale, controlling the pore size (20 to 80 nm), the surface-to-volume ratio of the mesoporous structure, as well as the three-dimensional connectivity of the "skeleton" and pore phases. The "carbon scaffold"-forming properties of PI also enabled us to extend TiO_2 crystallization to higher temperatures without loss of porosity, thereby facilitating mainly anatase crystal formation and enhancing the ensuing solar cell performance, which was maximized for films heated to 550 °C. We also found the material best suited to solid-state DSC operation when fine-tuning the titania precursor content and polymer molecular weight, resulting in films with a highly open porous structure consisting of pore sizes of the order of 30 nm. Our study demonstrates the flexibility of using diblock copolymers as structure directing agents for the creation of customized mesopore morphologies for optoelectronic and electrochemical applications.

2 Experimental

Mesoporous TiO_2 films were synthesized as follows: PI-*b*-PEO block copolymers with molecular weights M_n = 15.5 kg mol^{-1}, M_n = 33.5 kg mol^{-1}, and M_n = 84.4 kg mol^{-1} with PEO weight fractions of 0.23, 0.23, and 0.14, respectively, were dissolved in anhydrous tetrahydrofuran (THF). $TiCl_4$ and Ti-isopropoxide (Aldrich) were added and the solution stirred for 2 h.[15]

The titania precursors selectively swell the PEO domains of the block copolymer morphology, thereby modifying the polymer phase morphology.[10] For the polymer to inorganic precursor mass ratios between 5:2 and 1:2 used in this study, PI minority domains in a swollen matrix of PEO/inorganic were obtained. Qualitatively, the polymer-precursor ratio controls the porosity of the resulting TiO_2 network. Thin films were spin-cast onto fluorine doped SnO_2 (FTO) coated glass slides (15 Ω/□, TEC 15, Nippon Sheet Glass). The film thicknesses varied between 300 nm and 1 μm per spin-coated layer, depending on the molecular weight of the diblock copolymer, the amount of titania precursor, and the solution concentration. After spin-coating, the films were placed on a hot plate set to 100 °C for 1 h to evaporate all volatiles. They were then transferred into a tube furnace for heat treatment (450–600 °C) for 2 h in an inert atmosphere (N_2 or Ar). During this stage PEO is burnt off and PI is transformed into a sturdy amorphous graphitic-like carbon supporting the pore cavities. To remove the carbon, the samples were subsequently heated in oxygen at 500 °C for 1 h. Prior to device fabrication, some of the TiO_2 films were characterized by wide angle X-ray powder diffraction (XRD) and scanning electron microscopy (SEM).

Solid-state dye-sensitized solar cells were assembled as follows: the porous TiO_2 films were immersed in a mild piranha solution (1 part Millipore water, 3 parts sulfuric acid, and 2 parts hydrogen peroxide) for 30 minutes at 50 °C, rinsed in Millipore water and ethanol and dried in a N_2 flow. The TiO_2 films were subsequently soaked in a 3 × 10^{-4} M dye solution of amphiphilic polypyridyl ruthenium complex, cisRuLL'(SCN)^2 (L = 4,4'-dicarboxilic-acid-2,2'bipyridine, L' = 4,4'-dinonyl-2,2' bipyridine) (Z907) in acetonitrile:tert-butanol (1:1 vol%) at room temperature.[16] The hole transporting material used for these devices was 2,2',7,7'-tetrakis (N,N-di-methoxypheny-amine)-9,9'-spirobifluorene (spiro-MeOTAD) dissolved in

chlorobenzene (180 mg ml^{-1}) and mixed with Li[CF_3SO_2]$_2$N, and tert-butylpyridine.[17] The dyed films were rinsed in acetonitrile and dried in air. The spiro-MeOTAD solution (20 μl) was deposited on top of the film and left for 40 seconds to penetrate into the pores prior to spin-coating. The top electrodes, consisting of a 150 nm thick silver layer, were deposited by thermal evaporation through a shadow mask.

The photovoltaic properties of the solar cells were probed by measuring the current–voltage characteristics in the dark and under simulated sun light calibrated to give the equivalent of AM 1.5 illumination at 100 mW cm^2. The calibration was performed using a Si reference cell purchased and calibrated at the Fraunhofer Institute of Solar Energy, with the mismatch factor calculated and applied over the entire active region of our test cells and the calibration diode. Transient photovoltage measurements were performed as previously described using a single red LED as both the perturbation and bias source.[7]

3 Results and discussion

In a first experiment we investigated the influence of the calcination temperature of the TiO_2 matrix upon mesopore formation and material crystallinity. A series of films were prepared on conducting glass substrates (FTO) using PI-*b*-PEO with a M_n = 15.5 kg mol^{-1} and a polymer to titania precursor ratio of 1:2 by mass. The films were heated at temperatures between 450 °C and 600 °C. Wide angle angle X-ray diffraction peaks of the four samples could all be assigned to anatase TiO_2 and FTO (Fig. 1a). Debye-Scherrer analysis of the (101) anatase peak is consistent with an average crystal size of ~13 nm for all temperatures. This is surprising because Choi *et al.* have reported a marked dependence of the crystal size on temperature in the 350–450 °C range.[18] The insensitivity of crystal size on annealing temperature suggests that either a steady state has been reached at 450 °C, or that the crystal size is controlled by the imposed constraints of the carbon scaffold. It was not possible to heat to higher temperatures on the glass substrates because of substrate softening. Powder samples annealed up to 800 °C showed a transition to the rutile phase at ~650 °C with a simultaneous growth in average crystal size to 25 nm at 800 °C accompanied by a loss in porosity. Fig. 1b shows a high-resolution transmission electron microscopy image of an anatase single crystal, from the material heated to 550 °C. A larger scale transmission electron micrograph of a similar synthesised TiO_2, shown in Fig. 1c, demonstrates the mesoporosity of this material. Note that the copolymer-derived TiO_2 was heated to the required temperature under an argon atmosphere for 2 hrs, followed by a temperature reduction to 500 °C (or maintaining the annealing temperature, if lower) prior to changing the atmosphere to oxygen to burn off the carbon residues. By following this protocol it was possible to retain mesoporosity in films annealed to 650 °C, which is not possible without the carbon scaffold that arises during anaerobic heating.[15]

Similar films, annealed in the 450 to 600 °C temperature range were tested in solid-state DSCs. They were first dyed in a solution of a bipyridyl ruthenim complex (termed Z907, dyesol) overnight. Although the films scattered light to a certain degree, the UV-vis absorption spectra were comparable for all samples, indicating comparable dye up-take and

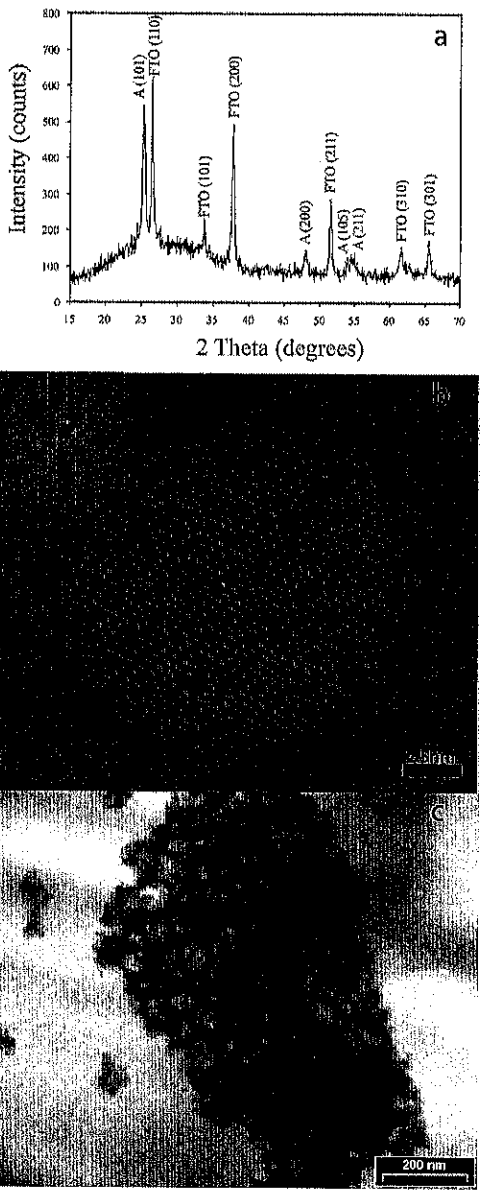

Fig. 1 (a) Wide angle X-ray diffraction spectrum of a porous TiO_2 layer annealed at 500 °C. All peaks are indexed to anatase titania (A) and FTO. (b) Lattice resolved HRTEM image of a single TiO_2 crystallite seen along the [100] zone axis, showing the hexagonal section of the particle and the low index plane termination of the surfaces. The inset shows the corresponding electron diffraction pattern. (c) TEM image showing similar mesostructured titania to that in (b). The samples were manufactured using PI-*b*-PEO of M_n = 15.5 kg mol^{-1} in a mass ratio to the titania precursor of 1:2.

roughness factors for the layers irrespective of the calcination temperature (data not shown). Solid-state DSCs were subsequently fabricated from these films and the current–voltage (J – V) curves measured under simulated sun light are shown in Fig. 2a. A marked increase in all the solar cell performance parameters is observed when increasing the TiO_2 processing temperatures from 450 °C to 550 °C: the open-circuit voltage V_{oc} increases from 0.65 V to 0.76 V, the short-circuit (J_{sc}) photocurrent from 0.71 mA cm^{-2} to 2.54 mA cm^{-2}, the fill

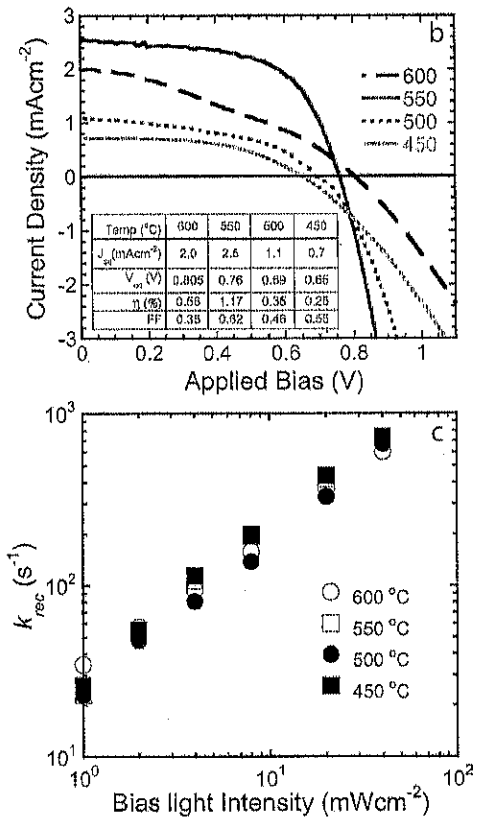

Fig. 2 (a) Photocurrent-voltage characteristics of solid-state DSCs fabricated from mesoporous TiO_2 films calcinated at temperatures between 450 °C and 600 °C. (b) Recombination rate constant, estimated from small perturbation open-circuit voltage decay measurements, as a function of bias illumination intensity for the four devices in (b). All films were manufactured using PI-*b*-PEO of $M_n = 15.5$ kg mol^{-1} in a mass ratio to the titania precursor of 1:2.

factor (FF) from 0.54 to 0.61, and most importantly the power conversion efficiency (η) improved from 0.25% to 1.2%. A further increase in TiO_2 processing temperature to 600 °C, resulted in a deterioration of device performance, mainly due to a drop in short-circuit current, although a further increase in V_{oc} is observed. The monotonic increase in the open-circuit voltage with increasing annealing temperature is most likely to be due to either a reduction in the charge recombination rate constant or to a reduction in the trap density-of-states beneath the conduction band, both of which would cause a greater splitting of the quasi Fermi levels under illumination. Fig. 2b shows the recombination rate constant, estimated from small perturbation open-circuit voltage decay measurements, as a function of bias illumination intensity for the four devices presented above. Interestingly, we observe very little difference as a function of processing temperature, suggesting that the increase in open-circuit voltage is predominantly due to a reduction in the defect site density. The drop in short-circuit current, fill factor and hence in efficiency when annealing at 600 °C may result from de-doping of the FTO electrode, introducing a current collection barrier, or increased series resistance. Furthermore 600 °C is close to the softening point of the glass potentially inducing extreme strain in the cooled films. Deriving the exact mechanism for this drop in performance at higher temperatures is beyond the scope of this work and the subject of further study.

In order to investigate the influence of the TiO_2 10 nm morphology on the solid-state DSC performance, we varied the parameters available through our fabrication technique: (1) a change in the copolymer molecular weight varies the inter-pore spacing and the pore diameter. (2) A variation in the precursor-to-polymer ratio (while also weakly affecting the pore spacing and diameter) controls the nature of the microphase morphology and, most importantly, the connectivity of the pores and the TiO_2 network.[10] Both parameters were systematically varied to investigate their influence upon the ensuing film morphology. Layers were made from all three polymers and for each system the polymer to precursor ratio was varied from 5:2 to 1:2 by mass and the samples were anaerobically heated to 550 °C for 1 h followed by 1 h in O_2 at 500 °C. SEM images of top views of the entire series and cryo-fractured side views of devices made from the PI-*b*-PEO sample series with $M_n = 15.5$ kg mol^{-1} are shown in Fig. 3.

Superficial examination of the images confirms the expected variation of pore structure with polymer molecular weight: the pore diameter and spacing increases with polymer molecular weight. Decreasing the inorganic precursor content should increase the overall pore volume. While a small increase in apparent pore size with decreasing precursor content is visible for all three polymer molecular weights, there is also a noticeable reduction in the layer thickness, which is particularly noticeable for the samples with the lowest precursor content. For the series made from the polymer with $M_n = 15.5$ kg mol^{-1} in Fig. 3(b), for example, the film thickness decreases only weakly (from 860 nm to 720 nm) when decreasing the amount of added titania precursor (*i.e.* when increasing the polymer to precursor mass ratio) from 1:2 to 1:1. A further decrease to 5:2 leads to a significant thickness reduction to 320 nm. The apparent "structural collapse" for the low titania content may therefore counteract to some extent potential advantages of a more open pore structure in terms of pore connectivity and hole-transporter infiltration.

BET measurements were carried out to quantify the overall surface areas of the films. The pore volume (per sample mass) increased with decreasing precursor content (from 1:2 to 5:2 polymer to precursor mass ratio) for the structured titania films. For instance from 0.13 cm^3 g^{-1} to 0.19 cm^3 g^{-1} for the 15.5 kg mol^{-1} polymer and from 0.19 cm^3 g^{-1} to 0.45 cm^3 g^{-1} for the 33.5 kg mol^{-1} polymer. Assuming a density of 3.84 g cm^{-3} for anatase TiO_2, a pore volume of 0.45 cm^3 g^{-1} corresponds to the pores accounting for 64% of the total volume, *i.e.* a porosity of 64%.

Since the pore size determined by SEM changes only little with precursor content, the increase in pore content is the direct consequence of thinner pore walls (and interconnection struts), which result from a reduction of the mass of the titania scaffold. This is a clear indication that the structural properties of the porous titania are governed by the block copolymer self-assembly. Contrary to our expectations, the pore volume increased with increasing molecular weight for all precursor contents (*e.g.* from 0.19 cm^3 g^{-1} for the 15.5 kg mol^{-1} polymer to 0.4 cm^3 g^{-1} for the 84.4 kg mol^{-1} polymer, for the 2:3 polymer to precursor ratio).

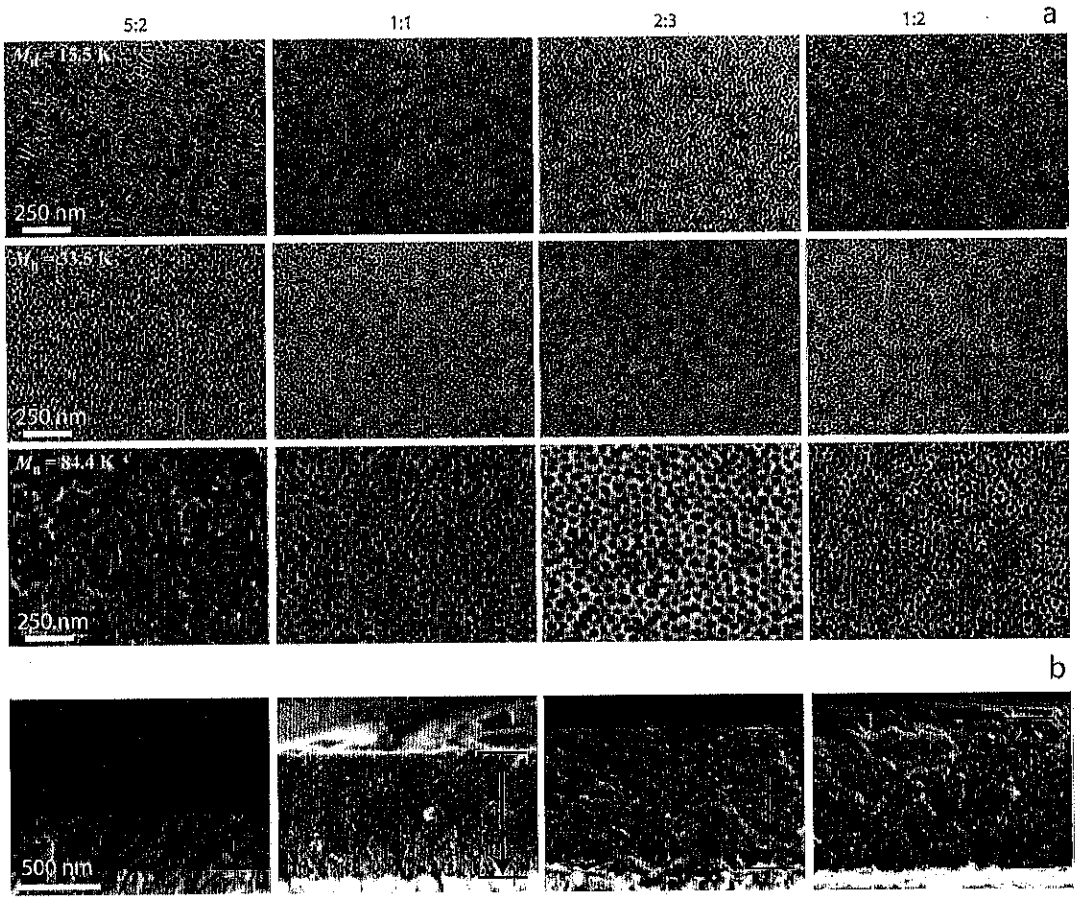

Fig. 3 (a) Top view SEM images of mesoporous TiO_2 films as a function of polymer PI-*b*-PEO molecular weight and precursor content. The polymer to titania precursor mass ratios are given in the column header. (b) Cross-sections of solid-state DSC devices made from the $M_n = 15.5$ kg mol^{-1} polymer. The thickness of the structured titania layer (indicated by arrows) decreases from 860 nm to 320 nm from right to left.

The reason for this increase in pore volume with molecular weight is not directly apparent. However, our analysis of the BET data[19] suggests that there are significant differences in the micro morphology as determined by differential nitrogen adsorption-desoption isotherms. Further investigation is currently underway to clarify this.

Solid-state DSCs were made from all samples imaged in Fig. 3 and their performance was compared. In Fig. 4a, the external quantum efficiency (EQE) is presented for the series based on the 15.5 kg mol^{-1} polymer. The samples tended to scatter light somewhat due to macroscopic inhomogeneity in the films, making light absorption measurements difficult. However, there generally seemed to be little difference in terms of light absorption between the samples. The BET surface area estimations were approximately constant with varying titania content at around 30 m^2 g^{-1} for these samples.

Fig. 4b compares the performance of devices made with the 15.5 kg mol^{-1} and 33.5 kg mol^{-1} polymers, both made with a 1:1 polymer to precursor mass ratio. While the open-circuit voltages and fill factors for the two devices are similar, the 650 nm thick device made with the 33.5 kg mol^{-1} polymer has a higher short-circuit current and therefore a higher power conversion efficiency of $\eta = 1.50\%$ compared to the 720 nm thick device made with the 15.5 kg mol^{-1} polymer with $\eta = 1.25\%$. It is most likely that this difference results from the improved open pore structure of the larger meso-morphology, enabling enhanced dye loading and hole-transporter infiltration, as indicated by the BET measurements (estimated surface area: 40 m^2 g^{-1} for the 33.5 kg mol^{-1} sample as compared to 30 m^2 g^{-1} for the 15.5 kg mol^{-1} sample).

We did not succeed in making equivalent devices from titania structured with the 84.4 kg mol^{-1} polymer. Unexpectedly, the larger pore size of this material prevented wetting of the films with the spiro-MeOTAD solution, making it impossible to coat, let alone infiltrate with the hole-transporter.

We note that the power conversion efficiencies reported here are considerably lower than the optimized state-of-the-art, where efficiencies of up to 4% are achieved with this dye and over 5% with an improved sensitizer.[7,20] In the present study, the thicknesses of the active layers are only on the order of 700 nm as compared to 2 μm for the best performing devices described in the literature. Unfortunately, attempts to fabricate thicker films have proved challenging due to the appearance of cracks and film instabilities. However, when compared to state-of-the-art films of similar thicknesses employing a similar dye to that used here, the efficiencies are comparable.[21] Furthermore, this represents a first investigation into controlling the titania morphology in this fashion when applied to solid-state DSCs, and we expect

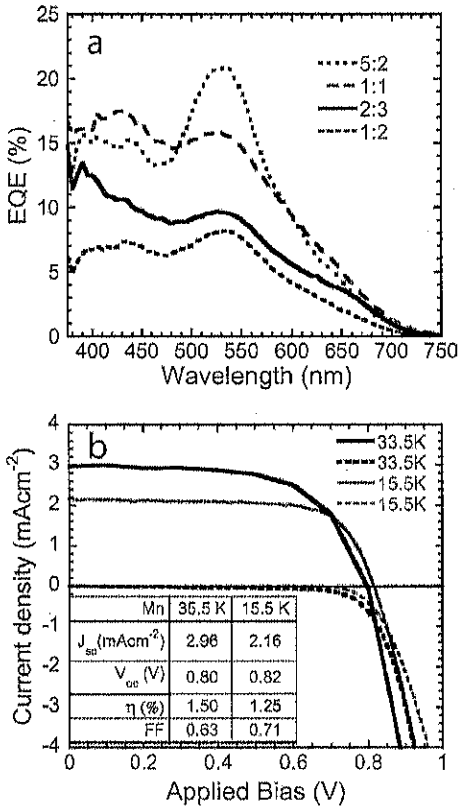

Fig. 4 (a) External quantum efficiency (EQE) action spectra for devices made with 15.5 kg mol^{-1} Pi-*b*-PEO, as a function of precursor content. (b) Photocurrent-voltage characteristics for solid-state DSCs based on the 33.5 kg mol^{-1} copolymer (red) in comparison to a similar device made using the 15.5 kg mol^{-1} polymer. Both samples had a 1:1 polymer to precursor weight ratio. The solid lines correspond to a measurement under simulated AM 1.5 full sun light illumination (100 mW cm^{-2}). The dashed lines show the dark current.

considerable improvement through refining the material fabrication protocol, surface structure and morphology control.

4 Conclusion

In summary, we have employed PI-*b*-PEO copolymers as structure directing agents for the synthesis of mesoporous TiO_2, with the ensuing films employed as mesostructured electrodes in solid-state dye-sensitized solar cells. This system provides detailed structural control on the mesoscopic length scale, which is crucial for optimizing the solar cell performance. We have demonstrated that the characteristic feature length scale can be controlled by altering the molecular weight of the polymer, and that the morphological structure can be controlled by altering the titania-to-polymer composition. We have found for our system that the solar cell performance is maximized when the characteristic length scale is of the order of 30 nm in an open highly-porous film. Furthermore, the versatility of the porous inorganic film formation method employed here is rather generic and may allow the synthesis of other inorganic semiconductors, thereby enabling the facile creation of a materials library for hybrid photovoltaics. The demonstrated detailed structural control combined with wide range of accessible semiconducting materials should increase our understanding of the role of nanostructures in photovoltaic devices and thereby ultimately lead to a significant improvements in performance.

5 Acknowledgements

M. N., S. H., and U. S. acknowledge financial support from the European network "PolyFilm" under RTN-6. This work was in part funded by EPSRC, NSF (DMR-0404195) and KAUST. The sabbatical leave of U. W. was supported by the Leverhulme Trust and EPSRC. C. D. acknowledges the Royal Society for Funding. We thank Richard Friend for support.

References

1 P. Yang, D. Zhao, D. I. Margolese, B. F. Chmelka and G. D. Stucky, *Nature*, 1998, **396**, 152.
2 B. Tian, X. Liu, B. Tu, C. Yu, J. Fan, L. Wnang, S. Xie, G. D. Stucky and D. Zhao, *Nat. Mater.*, 2003, **2**, 159.
3 B. O'Regan and M. Grätzel, *Nature*, 1991, **353**, 737.
4 U. Bach and M. Grätzel, *Nature*, 1998, **395**, 583.
5 D. Poplavskyy and J. Nelson, *J. Appl. Phys.*, 2003, **93**, 341.
6 L. Schmidt-Mende and M. Grätzel, *Thin Solid Films*, 2006, **500**, 296.
7 H. J. Snaith, A. J. Moule, C. Klein, K. Meerholz, R. H. Friend and M. Grätzel, *Nano Lett.*, 2007, **7**, 3372.
8 K. D. Benkstein, N. Kopidakis, J. van de Lagemaat and A. J. Frank, *J. Phys. Chem. B*, 2003, **107**, 7759.
9 N. Kopidakis, N. R. Neale, K. Zhu, J. van de Lagemaat and A. J. Frank, *Appl. Phys. Lett.*, 2005, **87**, 202106.
10 M. Templin, A. Frank, A. Du Chesne, H. Leist, Y. Zhang, R. Ulrich, V. Schädler and U. Wiesner, *Science*, 1997, **278**, 1795.
11 D. Zhao, Q. Huo, J. Feng, B. F. Chmelka and G. D. Stuckey, *J. Am. Chem. Soc.*, 1998, **120**, 6024.
12 K. M. Coakley and M. D. McGehee, *Appl. Phys. Lett.*, 2003, **83**, 3380.
13 K. M. Coakley, Y. Liu, M. D. McGehee, K. L. Frindell and G. D. Stucky, *Adv. Funct. Mater.*, 2003, **13**, 301.
14 M. Zukalova, A. Zukal, L. Kavan, M. K. Nazeeruddin, P. Liska and M. Grätzel, *Nano Lett.*, 2005, **5**, 1789.
15 J. Lee, M. C. Orilall, S. C. Warren, M. Kamperman, J. F. DiSalvo and U. Wiesner, *Nat. Mater.*, 2008, **7**, 222.
16 L. Schmidt-Mende, S. M. Zakeeruddin and M. Grätzel, *Appl. Phys. Lett.*, 2005, **86**, 013504.
17 H. J Snaith, L. Schmidt-Mende, M. Chiesa and M. Grätzel, *Phys. Rev. B*, 2006, **74**, 045306.
18 S. Y. Choi, M. Mamak, S. Speakman, N. Chopra and G. A. Ozin, *Small*, 2005, **1**, 226.
19 A. W. Marczewski, *A Practical Guide to Isotherms of Adsorption on Heterogeneous Surfaces*, http://adsorption.org/awm/ads/Ads.htm.
20 L. Schmidt-Mende, S. M. Zakeeruddin and M. Grätzel, *Appl. Phys. Lett.*, 2005, **86**, 01354.
21 H. J. Snaith and M. Grätzel, *Adv. Mater.*, 2007, **19**, 3643.